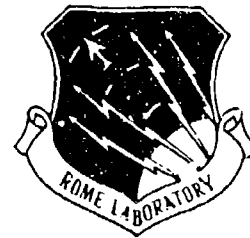


RL-TR-94-154  
Final Technical Report  
August 1994



AD-A285 795

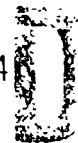


# OPTICAL IMAGE CORRELATOR USING ORTHOGONAL DATA STORAGE

Accuwave

Koichi Sayano and George A. Rakuljic

OTIC  
FILED  
OCT 27 1994



*APPROVED FOR PUBLIC RELEASE; DISTRIBUTION UNLIMITED.*

94-33334



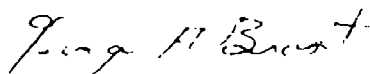
Rome Laboratory  
Air Force Materiel Command  
Griffiss Air Force Base, New York

94 10 26 024

This report has been reviewed by the Rome Laboratory Public Affairs Office (PA) and is releasable to the National Technical Information Service (NTIS). At NTIS it will be releasable to the general public, including foreign nations.

RL-TR-94-154 has been reviewed and is approved for publication.

APPROVED:



GEORGE A. BROST  
Project Engineer

FOR THE COMMANDER:



DONALD W. HANSON  
Director of Surveillance & Photonics

If your address has changed or if you wish to be removed from the Rome Laboratory mailing list, or if the addressee is no longer employed by your organization, please notify RL ( OCPA ) Griffiss AFB NY 13441. This will assist us in maintaining a current mailing list.

Do not return copies of this report unless contractual obligations or notices on a specific document require that it be returned.

REPORT DOCUMENTATION PAGE			Form Approved OMB No 0704-0188	
<small>Public reporting burden for this collection of information is estimated to average 1 hour per response, including the time for reviewing instructions, searching existing data sources, gathering and maintaining the data needed, and completing and reviewing the collection of information. Send comments regarding this burden estimate or any other aspect of this collection of information, including suggestions for reducing this burden, to Washington Headquarters Services, Directorate for Information Operations and Reports, 1215 Jefferson Davis Highway, Suite 1204, Arlington, VA 22202-4302, and to the Office of Management and Budget, Paperwork Reduction Project (0704-0188), Washington, DC 20503.</small>				
1. AGENCY USE ONLY (Leave Blank)		2. REPORT DATE August 1994		3. REPORT TYPE AND DATES COVERED Final Mar 93 - May 94
4. TITLE AND SUBTITLE OPTICAL IMAGE CORRELATOR USING ORTHOGONAL DATA STORAGE			5. FUNDING NUMBERS C - F30602-93-C-0021 PE - 62702F PR - 4600 TA - P1 WU - P1	
6. AUTHOR(S) Koichi Sayano and George A. Rakuljic				
7. PERFORMING ORGANIZATION NAME(S) AND ADDRESS(ES) Accuwave 1651 19th Street Santa Monica CA 90404			8. PERFORMING ORGANIZATION REPORT NUMBER  N/A	
9. SPONSORING/MONITORING AGENCY NAME(S) AND ADDRESS(ES) Rome Laboratory (OCPA) 25 Electronic Pky Griffiss AFB NY 13441-4515			10. SPONSORING/MONITORING AGENCY REPORT NUMBER  RL-TR-94-154	
11. SUPPLEMENTARY NOTES  Rome Laboratory Project Engineer: George A. Brost/OCPA/(315) 330-7669				
12a. DISTRIBUTION/AVAILABILITY STATEMENT  Approved for public release; distribution unlimited.			12b. DISTRIBUTION CODE	
13. ABSTRACT (Maximum 200 words)  A compact optical image correlator using orthogonal, wavelength multiplexed Fourier transform holograms recorded in a photorefractive crystal has been demonstrated. Cross-correlation and auto-correlation measurements were obtained using randomly selected test images against the set of reference images stored in the orthogonal data storage volume hologram. Over 40 holograms were written in the 645 to 651 nm wavelength range with >2% diffraction efficiency and 1.5 Å wavelength separation. A low power tunable external cavity semiconductor laser was used for readout, further demonstrating the portability of this approach. The input image translation tolerances on the correlation output and the effect of using partial images during readout were also investigated.				
14. SUBJECT TERMS Optical image correlation, Pattern recognition, Optical memory, Volume holography, Optical data storage			15. NUMBER OF PAGES 40	
			16. PRICE CODE	
17. SECURITY CLASSIFICATION OF REPORT UNCLASSIFIED	18. SECURITY CLASSIFICATION OF THIS PAGE UNCLASSIFIED	19. SECURITY CLASSIFICATION OF ABSTRACT UNCLASSIFIED	20. LIMITATION OF ABSTRACT SAR	

# **OPTICAL IMAGE CORRELATOR USING ORTHOGONAL DATA STORAGE**

## **Final Technical Report**

### **INTRODUCTION**

Optical image correlation is an important application with numerous military and military/commercial dual-use applications, among them being pattern and target recognition, object and document identification, and image processing.<sup>1,5</sup> Optical implementation of this operation, where the correlation between the input and reference images is obtained by using optically-generated Fourier transforms, enables the result of this very complex (and computation-intensive) mathematical operation to be obtained instantaneously. In addition, when this approach is coupled with volume holographic optical memories that store the reference templates for comparison with the unknown input images, additional advantages of high density storage and parallel readout are also realized.

The work at Accuwave Corporation in collaboration with the Photonics Center of Rome Laboratory during the past year under this Expert Science and Engineering program has shown the feasibility and advantages of incorporating orthogonal data storage volume holography as the storage mechanism for an all-optical image correlator. The high spatial resolution feature of orthogonal data storage is used in an advantageous manner by storing Fourier transforms of various images, which inherently have high resolution spatial features, in a photorefractive crystal with reduced crosstalk and wavelength multiplexing.

The primary advantages of orthogonal data storage, i.e. high storage densities with reduced crosstalk and sidelobe levels, have been demonstrated under previous programs, i.e. with ARPA, and the results and analysis have been published in the literature. Data storage experiments have demonstrated the capability of storing at least 100 images with feature sizes as small as  $2\text{ }\mu\text{m}$  with sufficient signal to noise ratio for readout with a CCD camera. In this program, this technology was extended to storing Fourier transform holograms for image correlation. Wavelength multiplexing is used to access the different "pages" of holograms, which also provides a means for rapid scanning through the entire set of stored images.

A breadboard optical correlator was constructed and demonstrated both at Accuwave and Rome Laboratory. The holograms of the reference images were written at Accuwave in a 4 mm thick  $\text{LiNbO}_3$  crystal using a single-frequency dye laser. For readout, the dye laser was used at Accuwave, while a tunable (visible) external cavity semiconductor laser was used in the demonstration at Rome Laboratory. The latter shows the portability potential of this system. The auto- and cross-correlations of various images were obtained to characterize the performance of the correlator system are further described later in this report. Translation invariance and readout with partial images were also investigated.

## **TECHNICAL APPROACH**

Optical correlation is a fundamental operation of pattern recognition, where an unknown input image is to be compared against a set of stored references in order to identify and/or classify it. Although most experiments have used images of the targets,

the more general definition of the "image" is any array of patterns, grey levels, or vectors representing sensory inputs. In the all-electronic implementation, the input is digitized by a CCD array and a computer used to generate the correlation against stored reference images. The drawback of this scheme is the amount of computing time required to evaluate the correlation integrals, especially if the input image has many pixels and must be compared against a large number of reference images.

### OPTICAL IMAGE CORRELATION

Figure 1 illustrates a block diagram of the fundamental approach for image correlation systems, where the correlation between an unknown input image and each of a large number of stored reference images is computed to identify the unknown image.<sup>6</sup> This approach is based on multiplying the (two-dimensional) Fourier transforms of the two images and taking the inverse Fourier transform of the product, which is the definition of correlation as shown below:<sup>7</sup>

$$\begin{aligned} h(x,y) &= FT^{-1} \left[ F^*(k_x, k_y) G(k_x, k_y) \right] \\ &= \frac{1}{(2\pi)^2} \int_{-\infty}^{\infty} \int_{-\infty}^{\infty} F^*(k_x, k_y) G(k_x, k_y) e^{i(k_x x + k_y y)} dk_x dk_y \\ &= f(x,y) * g(x,y) \end{aligned} \quad (1)$$

where  $F(k_x, k_y)$  and  $G(k_x, k_y)$  are the Fourier transforms of the image functions  $f(x,y)$  and  $g(x,y)$ , respectively:

$$\begin{aligned} F(k_x, k_y) &= FT[f(x,y)] = \int_{-\infty}^{\infty} \int_{-\infty}^{\infty} f(x,y) e^{-i(k_x x + k_y y)} dx dy \\ G(k_x, k_y) &= FT[g(x,y)] = \int_{-\infty}^{\infty} \int_{-\infty}^{\infty} g(x,y) e^{-i(k_x x + k_y y)} dx dy \end{aligned} \quad (2)$$

## OPTICAL CORRELATOR SYSTEM BLOCK DIAGRAM

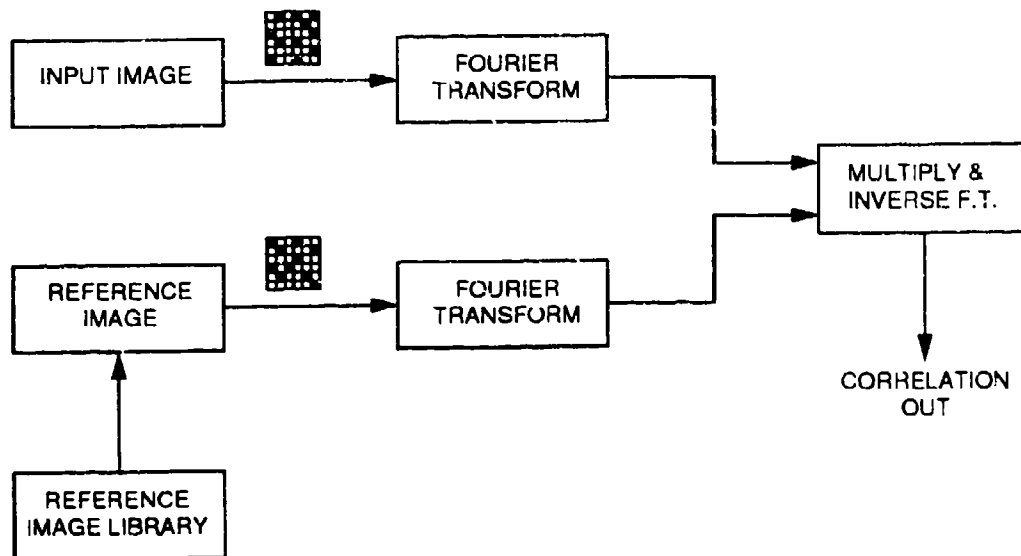


**FIGURE 1** Block diagram of the approach used for optical image correlation, where optically-generated Fourier transforms of the input and reference images are multiplied and inverse Fourier transformed to obtain the correlation. Random binary patterns as well as images can be used in this system.

The advantage of an optically-based correlator system is that the Fourier transform and its inverse can be generated instantaneously using a converging lens placed one focal length from the object and image planes. A correlator system utilizing this approach is shown in Figure 2, where the input image is Fourier transformed optically and multiplied with the Fourier transform of the reference image, which is loaded into the spatial light modulator. The product is then inverse Fourier transformed by the second lens onto the output plane to obtain the correlation.

This approach was used for the original in-house correlator program at Rome Laboratory, using two SLM's for the input and reference images.<sup>1</sup> The reference Fourier transform templates were computed and stored in the computer. To compute the correlation of an input image in the first SLM with a stored reference image, the Fourier transform was downloaded directly from the computer onto the SLM. Although the Fourier transform of the input image is obtained instantaneously, the disadvantage of this approach is the length of time required to sequentially download all of the stored (Fourier transform) reference images to the SLM. This delay can be significant for a large number of stored images, and it also increases with higher pixel resolution.

For this program, the configuration of Figure 2 was used as a starting point, with the second spatial light modulator replaced by a reflection mode volume hologram. This change also eliminated the need for the second Fourier transform lens in the system. Note that the orthogonal data storage configuration, with its exact retro-reflecting geometry, is well suited for this application.<sup>8-10</sup> The approach is shown in Figure 3, where Fourier transform holograms are stored in the photorefractive crystal with plane reference

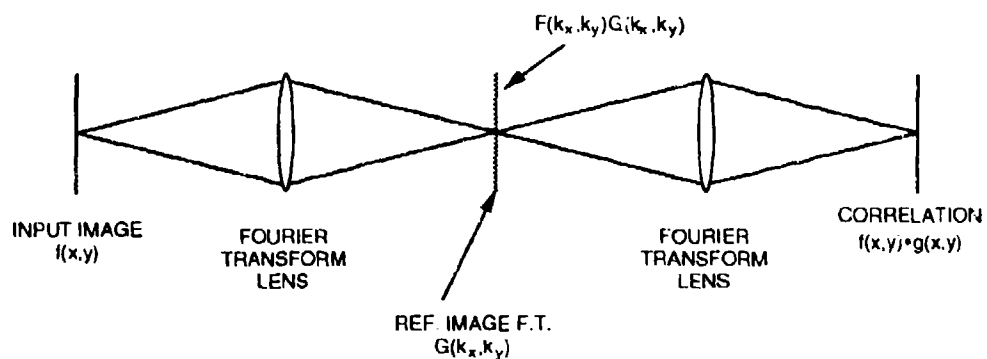
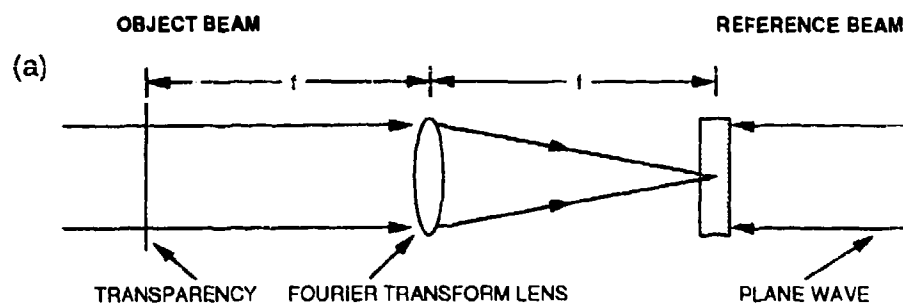


FIGURE 2 Schematic diagram of the  $4F$  optical correlator using two spatial light modulators.

#### RECORDING



#### READOUT

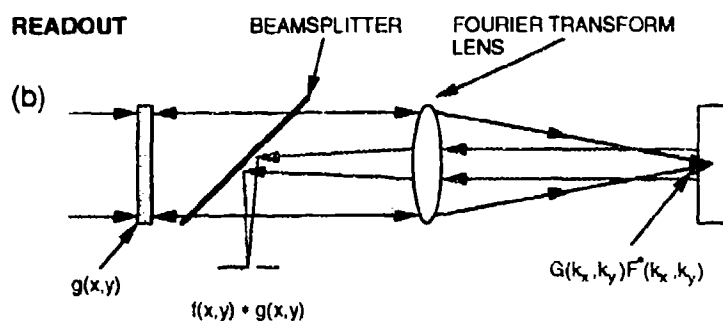


FIGURE 3 Diagram showing use of the orthogonal data storage holographic memory as the storage element in the optical image correlator.

beams to serve as the reference images. Wavelength is used to address specific holograms stored in the crystal. During readout, the unknown image to be identified is Fourier transformed by the lens and used to illuminate the hologram. The product of the Fourier transforms of the input and reference images is reflected back through the lens to obtain the correlation. Since the correlation is computed instantaneously, the system can scan through wavelength very quickly, limited only by the tuning speed of the source.

### ORTHOGONAL DATA STORAGE

The advantage of orthogonal data storage lies in the reduced holographic crosstalk between adjacent "pages" of data, therefore allowing higher data densities and therefore increased capacity.<sup>9,10</sup> Recent work by others have also validated these advantages in the applications of optical data storage and image correlation.<sup>11,12</sup>

The reduced crosstalk in orthogonal data storage arises from the uniform distribution of the recorded information in the grating  $\mathbf{K}$ -space as well as the physical volume of the medium.<sup>9</sup> A recorded grating vector, given by

$$\mathbf{K} = \mathbf{k}_{obj} - \mathbf{k}_{ref} \quad (3)$$

can be identified by the point  $(K_x, K_y, K_z)$  in  $\mathbf{K}$ -space. The image-bearing object beam (i.e. a spatially modulated plane wave) can be decomposed into an angular spectrum of plane waves, so for an information-bearing hologram, the locus of points becomes a surface extending over angle  $\varphi$ , as shown in Figure 4(a). As the locus of points for the grating wavevectors  $\mathbf{K}_{grating}$  get closer together, parasitic scattering off adjacent gratings causes increased crosstalk.

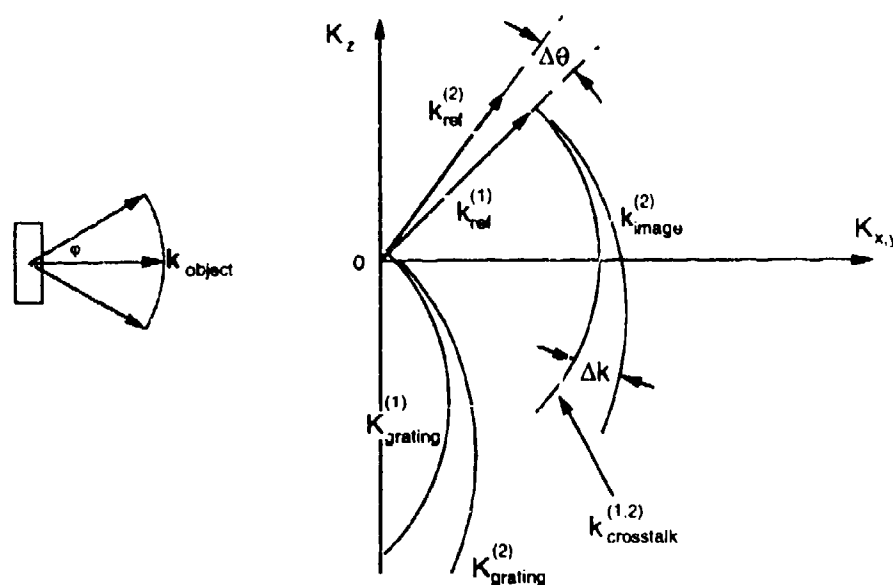


FIGURE 4(a) K-space diagram showing the source of crosstalk for high resolution, transmission mode gratings.

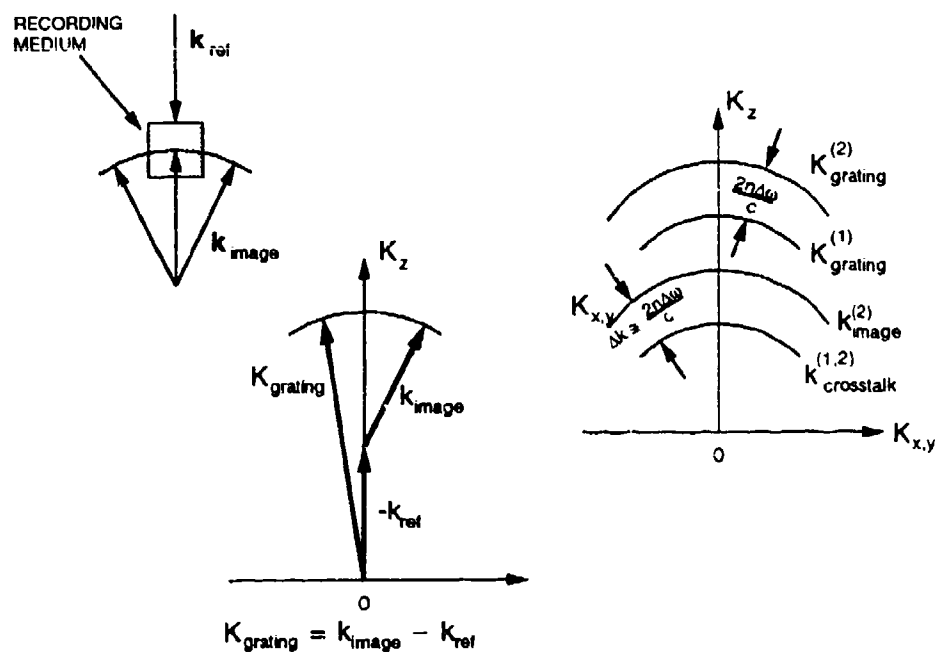


FIGURE 4(b) Corresponding K-space diagram for orthogonal data storage, where the counter-propagating geometry is used to obtain reduced crosstalk.

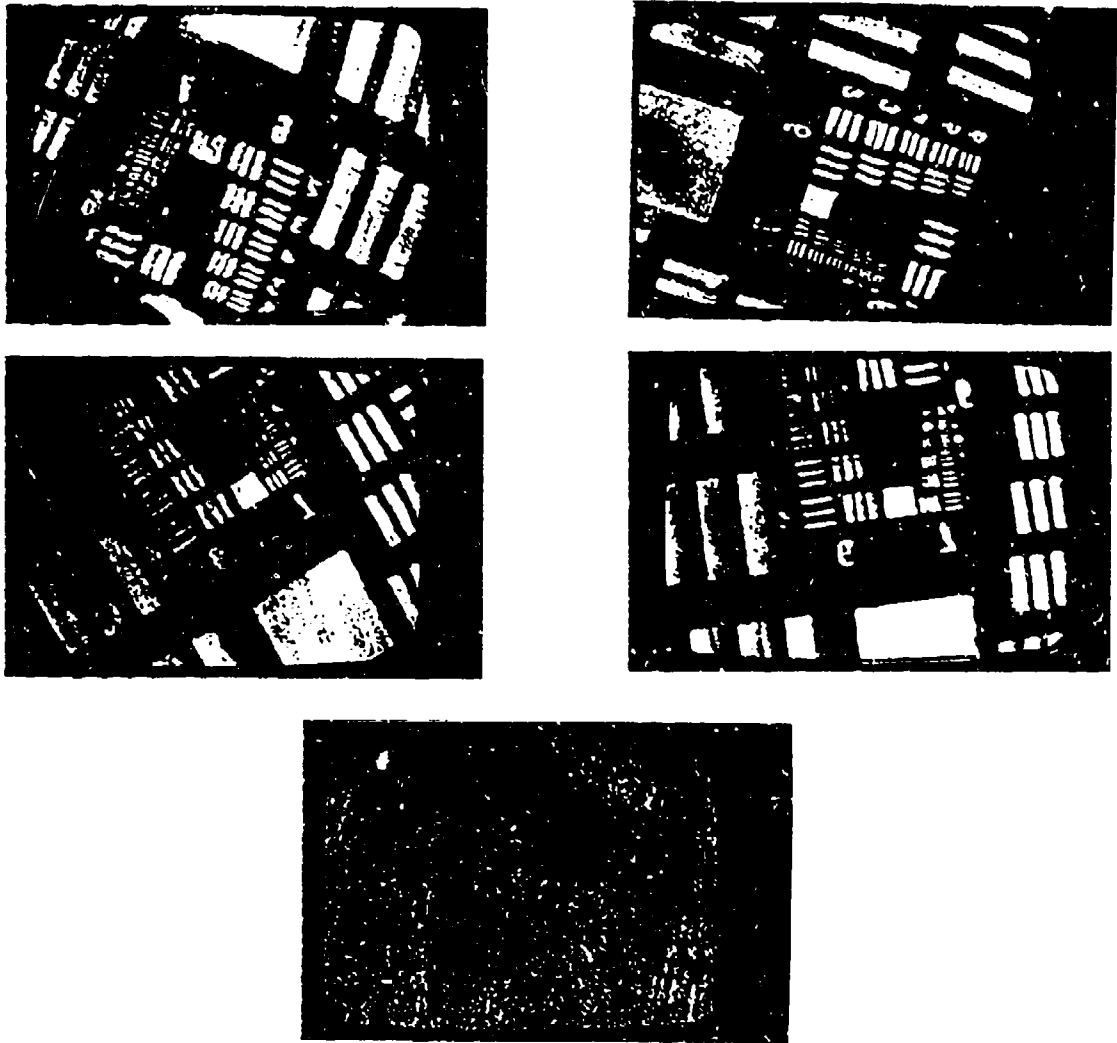


FIGURE 5 Selected images out of 100 high resolution holograms stored in a 4 mm thick  $\text{LiNbO}_3$  crystal using orthogonal data storage and 1.6 Å wavelength separation (top and middle); vacant wavelength address showing low crosstalk levels (bottom).

In orthogonal data storage, the object and reference beam orientations are  $180^\circ$  apart (i.e. counterpropagating), so the information content of the object beam is spread laterally in **K**-space. Wavelength multiplexing is used to separate adjacent pages of data, so the separation in **K**-space between holograms is nearly uniform and independent of the information content, as shown in Figure 4(b). Therefore, even for very high resolution holograms, the crosstalk is minimized.

These predictions were demonstrated by storing 100 holograms of a high resolution image (with  $< 2 \mu\text{m}$  spatial features) in a 4 mm thick medium using orthogonal data storage.<sup>10</sup> The images were wavelength multiplexed in the  $\text{LiNbO}_3$  crystal with approximately  $1.5 \text{ \AA}$  separation, and the image was incrementally rotated for each exposure so each hologram has an independent spatial distribution. Selected images from this experiment, along with a vacant intermediate wavelength address to illustrate the low crosstalk levels, are shown in Figure 5.

The orthogonal data storage configuration also results in maximum wavelength selectivity (or minimum bandwidth) and maximum angular field of view.<sup>13</sup> These qualities provide important advantages in storage applications, in particular the optical correlator implementation by providing increased storage densities as well as translation invariance.

For a reflection mode hologram at the Bragg condition, the reflected diffraction efficiency is given by<sup>14</sup>

$$\eta = \tanh^2 \left[ \frac{\pi n_1 l}{\lambda \cos \theta_0} \right] \quad (4)$$

where  $\theta_0$  is the Bragg incidence angle,  $l$  is the thickness,  $\lambda$  is the wavelength, and  $n_1$  is the index variation (which correlates with the coupling constant  $\kappa$ ).

Field of view, or the maximum angular deviation tolerated for Bragg reflection by a holographic grating, is at a maximum for orthogonal data storage. For unslanted reflection gratings with angle of incidence  $\theta$  and angular deviation  $\Delta\theta$ , the Bragg condition is given by<sup>14</sup>

$$2\pi \frac{n_0}{\lambda} \left[ \sqrt{1 - \frac{\cos^2(\theta - \Delta\theta)}{n_0^2}} - \sqrt{1 - \frac{\cos^2\theta}{n_0^2}} \right] = \frac{\pi}{l} \quad (5)$$

where  $\lambda$  is the wavelength (which is fixed in this case) and  $n_0$  is the index of refraction of the crystal (2.2 for LiNbO<sub>3</sub>). For example, for  $l = 4$  mm,  $\lambda = 650$  nm, and  $\theta = 0$ , the angular field of view is approximately  $2^\circ$ .

For transmission gratings, the field of view is considerably smaller than for orthogonal data storage, i.e. the counterpropagating reflection mode geometry. In the transmission geometry, the field of view  $\Delta\theta$  is given by<sup>14</sup>

$$\frac{2\pi}{\lambda} [\sin^2(\theta - \Delta\theta) - \sin^2\theta] = \frac{\pi}{l} \quad (6)$$

where the angle of incidence  $\theta$  for Bragg diffraction is measured relative to the normal to the incident surface. As a numerical example, for  $\theta = 45^\circ$  in the example described above, the field of view is  $0.0093^\circ$ , or  $34''$ .

Large field of view is especially advantageous in the optical correlator architecture used for this program by providing translation invariance in the position of the input

image. Changes in angle at the Fourier transform plane, where the holographic element is located, translate into positional variations at the input plane. Therefore, positional errors in the input image are accommodated by the large field of view of orthogonal data storage holograms. In contrast, the transmission geometry requires extremely precise angular positioning, which translates to tight tolerance requirements in the input image position.

## **EXPERIMENT DESIGN AND PLANNING**

The overall goal for this program was to integrate orthogonal data storage in the optical correlator experiment at Rome Laboratory. The plan was for the test images, or templates, to be recorded as orthogonal data storage in photorefractive LiNbO<sub>3</sub> crystals using the dye laser and holography facilities at Accuwave Corporation. Following initial experiments with this approach at Accuwave, a tunable external cavity semiconductor laser (which is located at Rome Laboratory) was used as the tunable readout source, demonstrating portability of the system. Testing and characterization of the correlator system was done at Rome Laboratory using their laser and data acquisition and image processing equipment.

### **EXPERIMENT DESIGN**

The configuration of the optical correlator breadboard and demonstration, based on the schematic diagram of Figure 3, is shown in Figure 6. A converging lens (which was an 85 mm focal length camera lens) was used to generate the Fourier transforms of the input image and reflected signal. The Fourier transform of the input image was used to illuminate the photorefractive crystal, so the product of it and the Fourier transform of

## OPTICAL CORRELATOR ARCHITECTURE

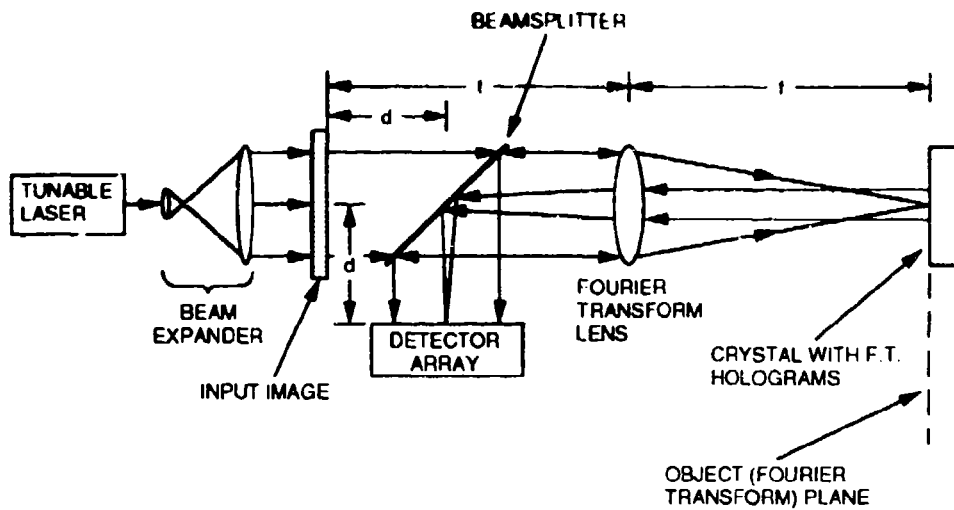


FIGURE 6 Configuration of the optical image correlator demonstration. A tunable external cavity semiconductor laser was used during readout.

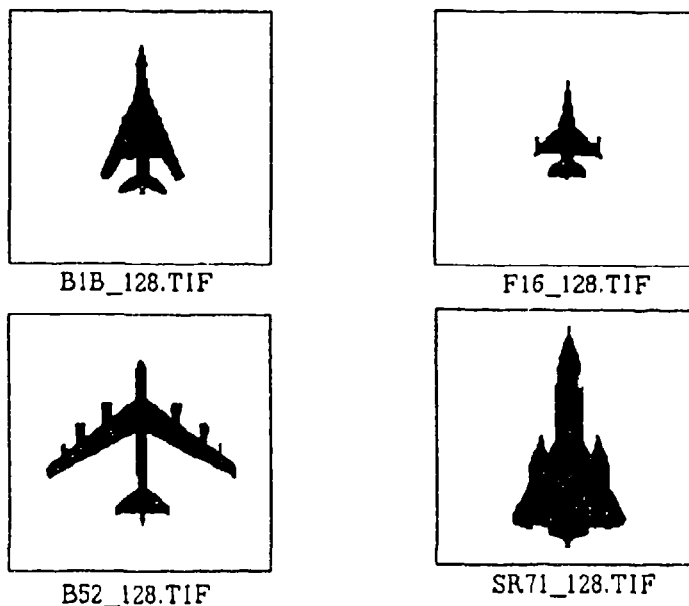


FIGURE 7 Image templates used as the reference and test images for the correlator demonstration. Each image is pixelized at  $128 \times 128$  density.

the reference is retro-reflected back through the lens. A beamsplitter was used to pick off the reflected signal and direct it onto a CCD camera.

Image templates of four aircraft silhouettes with sharply contrasting shapes (shown in Figure 7) were supplied by Rome Laboratory for use in this program. The initial plan that was proposed called for individual slides of different images (and images at different orientations to increase the number of distinct images) and a mechanical slide changer or similar mechanism to load the desired image in the input plane. However, in order to match field of view of the hologram with the pixel size of the image, a  $4\text{ mm} \times 4\text{ mm}$  image size was used (so pixel size was approximately  $30\text{ }\mu\text{m}$ ). The smaller image size also provides the advantage of allowing the multiple images to be arrayed on a single transparency, where a two-axis motion control system can then be used to position the correct image in the system. This allowed larger numbers of images to be used and reduced the cost of fabricating the image transparencies.

The images furnished by Rome Laboratory (which were binary with  $128 \times 128$  pixel resolution) were arranged in a rectangular array onto a single frame using the image processing and editing software at Rome Laboratory. The composite transparency had an array of 32 images, comprised of the four original images at eight different orientations. The images were reduced to  $4\text{ mm} \times 4\text{ mm}$  size, with an additional 2 mm guard band bordering all of the images. The entire array was then transferred onto a chrome-on-glass transparency to obtain high contrast. A Newport PMC-200 series PC-interfaced motion control system, with  $1\text{ }\mu\text{m}$  positioning accuracy, was used to move the selected image into position.

## FOURIER TRANSFORM HOLOGRAPHY DEVELOPMENT

Recording of Fourier transform holograms presents an entirely new set of technical issues compared to recording regular, high resolution images. In Fourier transform holography, the object beam is focused down with most of its power in a small, high intensity spot, so the intensity mismatch with the reference beam will result in lower grating amplitude. Moreover, the additional optical elements in the object beam path increase the probability for instabilities and unwanted path length fluctuations during the exposure.

Considerable effort was spent in developing the optical layout for writing and reading out the holograms. A schematic of the key optical elements of the correlator system during recording and readout was illustrated in Figure 6. The photograph in Figure 8 shows how these elements were mounted on the optical bench. The Fourier transform lens and crystal were mounted on an optical rail so the positions of these various elements can be recorded and reproduced. An 85 mm  $f/1.2$  camera lens was used for generating the Fourier transforms in this system. The camera lens, in addition to being near diffraction limited at a low  $f$ -number, also used multiple elements which shortened the actual focal distances from the front and back surfaces, decreasing the overall dimensions of the system.

Figure 9 illustrates the setup used for recording the holograms, where the ring geometry for the object and reference beams in the original orthogonal data storage recording experiments was retained to simplify alignment of the object and reference beams in a counterpropagating orientation. The optical rail-mounted components were

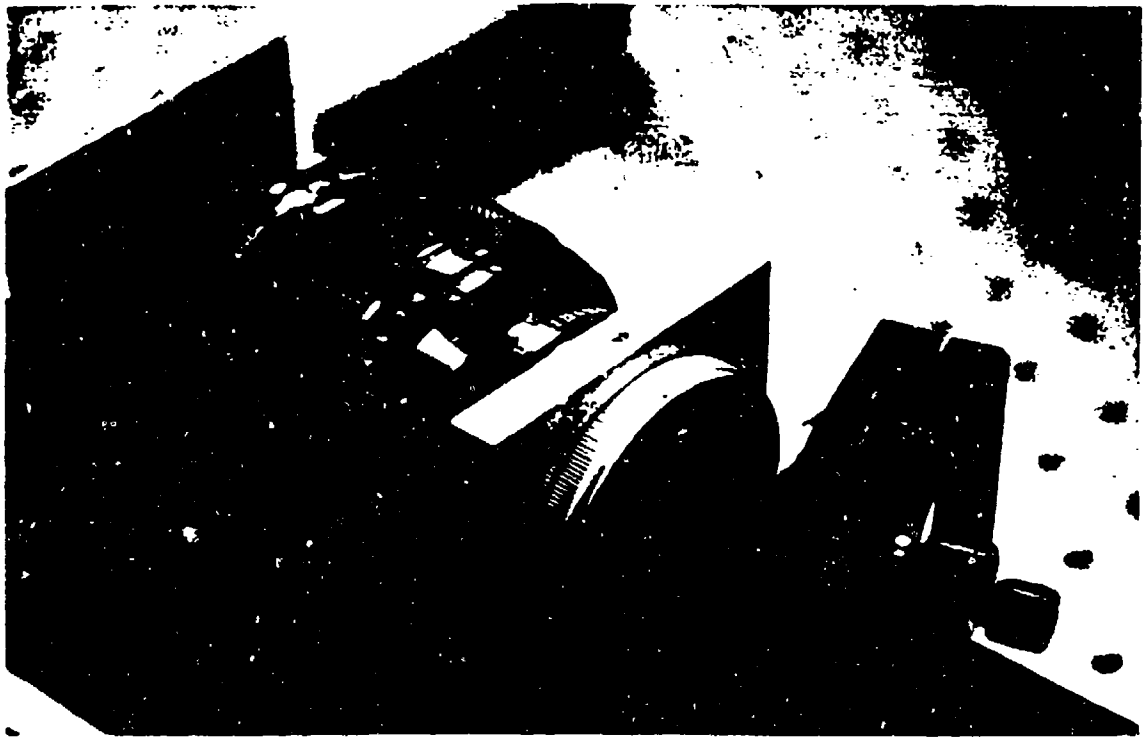


FIGURE 8 Photograph of the optical correlator breadboard.

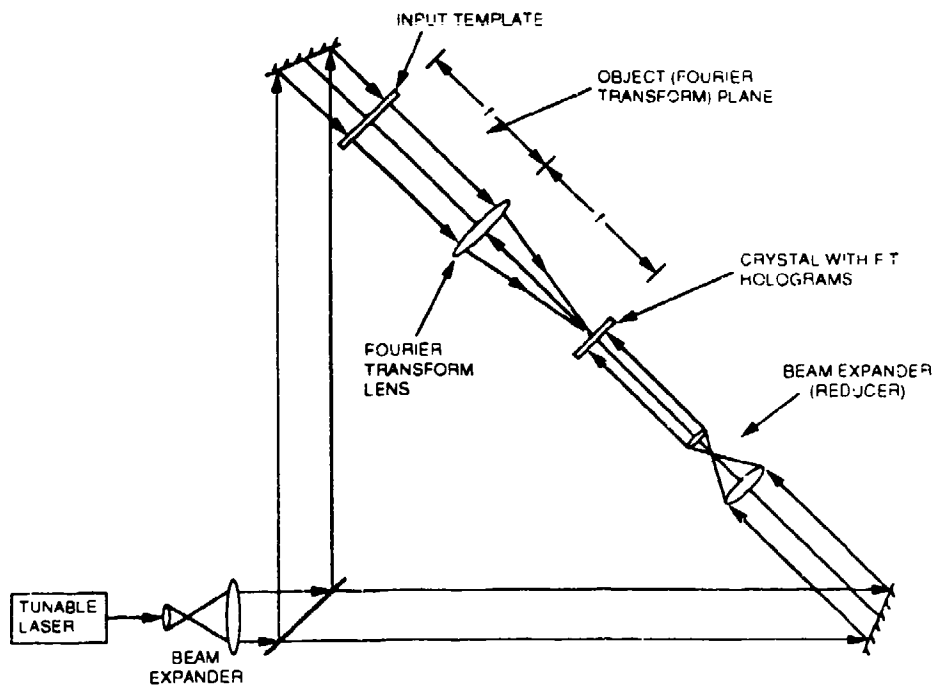


FIGURE 9 Optical layout of the correlator for recording the reference images in the photorefractive crystal.

positioned in one arm of the ring, with the crystal at the center to equalize the optical path lengths. The reference beam was directed from the opposite side in an exactly counterpropagating direction. A telescope was used to reduce the diameter of the reference beam to improve the intensity match with the object beam for a higher modulation index.

### SYSTEM DEMONSTRATION

After the holograms had been recorded at the holography laboratory of Accuwave Corporation, the correlator system was transported to Rome Laboratory for integration and testing with the tunable external cavity semiconductor laser, as planned in the original proposal. The image acquisition and processing systems at Rome Laboratory, including CCD cameras, frame grabbers, and image editing software, were also used in support of this program.

At the start of this program, Rome Laboratory ordered the tunable external cavity laser from Micracor, with the requirement that the center wavelength be as far to the blue as possible, preferably around 660 nm. This was to take advantage of having the operating wavelength closer to the peak of the DCM Special laser dye output and the increased photosensitivity of the crystal at shorter wavelengths, resulting in shorter writing time. The laser was to operate at  $660 \pm 15$  nm output at 25 mW peak power, but the actual delivered unit produced about 10 mW maximum power at the peak, which was below specifications. Moreover, a 670 nm optical head was the only one available at that time; the laser was scheduled to be retrofitted with the 660 nm head when it became available.

Despite the longer operating wavelength of the correlator, the  $\text{LiNbO}_3$  crystals used for this program had sufficient red photosensitivity to allow holograms to be recorded at 670 to 675 nm for the initial experiments. Therefore, the initial plan of testing the correlator system with the dye laser and operating using Rhodamine 6G dye (with 560 to 620 nm operation) was dropped in favor of doing all of the experiments using DCM Special (for operation at 620 to 690 nm). In the 4th Quarter of 1993, the laser was retrofitted with a new head for operation in the 642 to 656 nm band; in this wavelength range, the power available from the dye laser was much higher than at 670 nm, reducing the writing time by at least a factor of two for improved holography results and increased number of holograms.

## EXPERIMENTAL RESULTS

### FEASIBILITY DEMONSTRATION

After the transparency fabrication was completed, the correlator was set up on a 24"  $\times$  24" optical breadboard for the initial experiments. Both the writing and readout of the holograms were initially done with the dye laser, although the ultimate goal of the program was for the system to be tested with a tunable external cavity semiconductor laser for readout. Holograms were recorded using 670 nm light from the stabilized, single frequency dye laser, with the 3.2 Å modes of the thin etalon providing a convenient wavelength separation for the initial experiments.

For readout, the reference beam in the setup shown in Figure 9 was blocked and the original object beam was used for the readout illumination. This insured that the readout beam was properly Bragg-matched with the original object beam from the writing phase.

The motion controller was used to select the desired image, and the wavelength of the laser was scanned through the various wavelength addresses of the stored images to obtain the correlation. The auto-correlation, corresponding to the case where the stored image matches with the input image, gave a sharp peak (a delta function), while the cross-correlation (for mismatched images) had lower intensity and the features were diffused over a larger area.

### CORRELATOR TEST WITH TUNABLE EXTERNAL CAVITY LASER

The next step after demonstrating operation of the correlator with a dye laser was to incorporate the tunable external cavity semiconductor laser for readout. Holograms were recorded at Accuwave, then the correlator system was transported to Rome Laboratory for characterization using their tunable semiconductor laser and image acquisition equipment.

In the initial test, 7 holograms (of unique objects, i.e. the Rome Laboratory-supplied images) were stored in the 670 nm wavelength range at approximately 3 Å increments. An exposure schedule, where the sequential exposure times were decreased, was used to equalize the auto-correlation efficiencies of the holograms. Iris apertures were used to determine the correct position and incidence angle of the incoming object beam, so the same Bragg conditions could be reproduced when the system was dismantled for transport and later reassembled at Rome Laboratory.

The output of the Micracor laser was expanded using a 4× telescope and directed into the correlator with the proper orientation. The wavelength of the laser was registered by a Burleigh Wavemeter during readout. Since the laser output is in the form of

a stripe, part of the output power was lost by being cut off when the beam was expanded and passed through the input image transparency. The auto- and cross-correlations were observed as the semiconductor laser was tuned through all of the wavelength addresses for a given input image. Following the initial experiments, the laser was shipped back to the manufacturer for maintenance, repair, and installation of a new optical head for operation at shorter wavelengths.

With the new optical head, the laser's operating wavelength was shifted to the 642 to 657 nm range, where the available optical power for DCM Special dye was twice that of the 670 nm region. This resulted in more favorable conditions for holography, where short exposure times are critical to minimize the effects of vibration and drift. A piezoelectric cavity length control had also been added to the Micracor laser during this refurbishment, giving it an improved fine tuning capability compared to tuning with the grating alone.

Figures 10 and 11 illustrate the auto- and cross-correlation results obtained using the Micracor laser for readout. As can be seen from the figures, the auto- vs. cross-correlation is clearly discernable. The automatic gain control (AGC) on the camera was disabled, and the  $\gamma$  adjustment was set to 1 for a linear response. Peak auto-correlation efficiency was on the order of 2% for a total of 21 holograms stored in the crystal.

Up to 40 holograms were stored in a single volume (i.e. a 4 mm thick crystal) using this shorter wavelength range (around 650 nm). To record the 40 holograms, some of the images on the transparency were repeated and the wavelength addresses were positioned at 1.5 Å intervals for the 4 mm thick crystal (with 0.25 Å FWHM bandwidth).

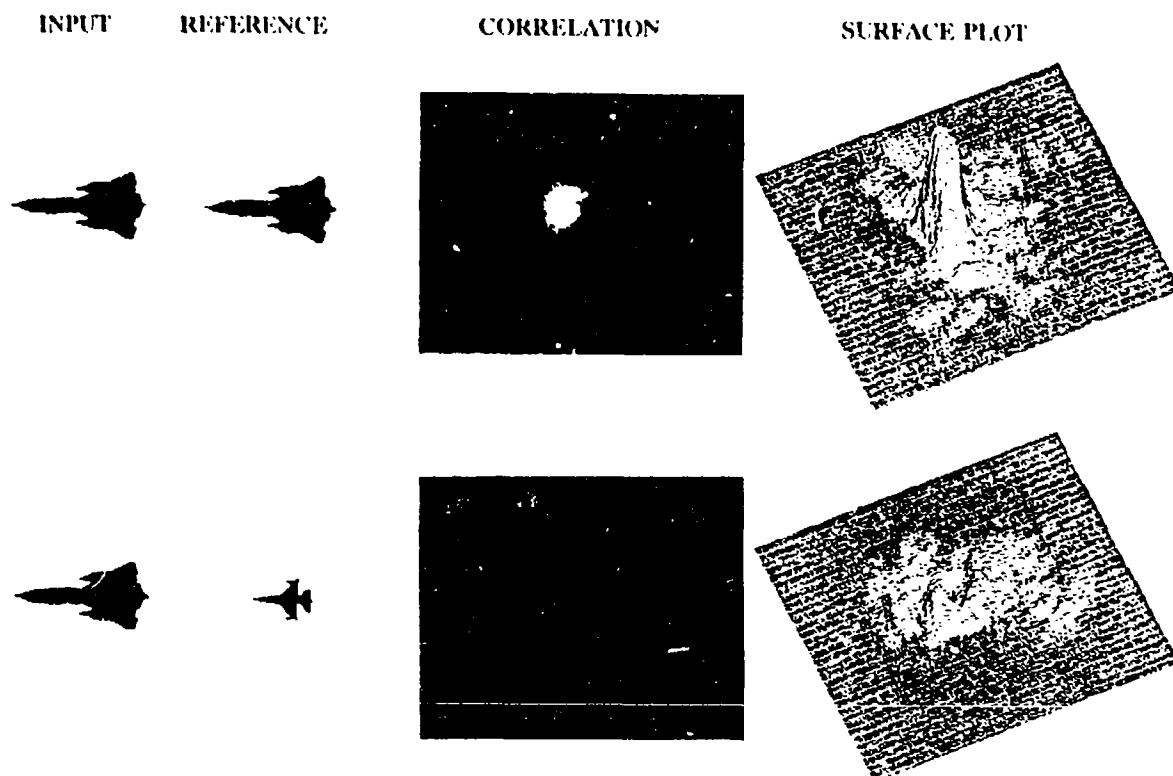


FIGURE 10 Results from the image correlation experiment, showing auto-correlation (top) and cross-correlation (bottom).

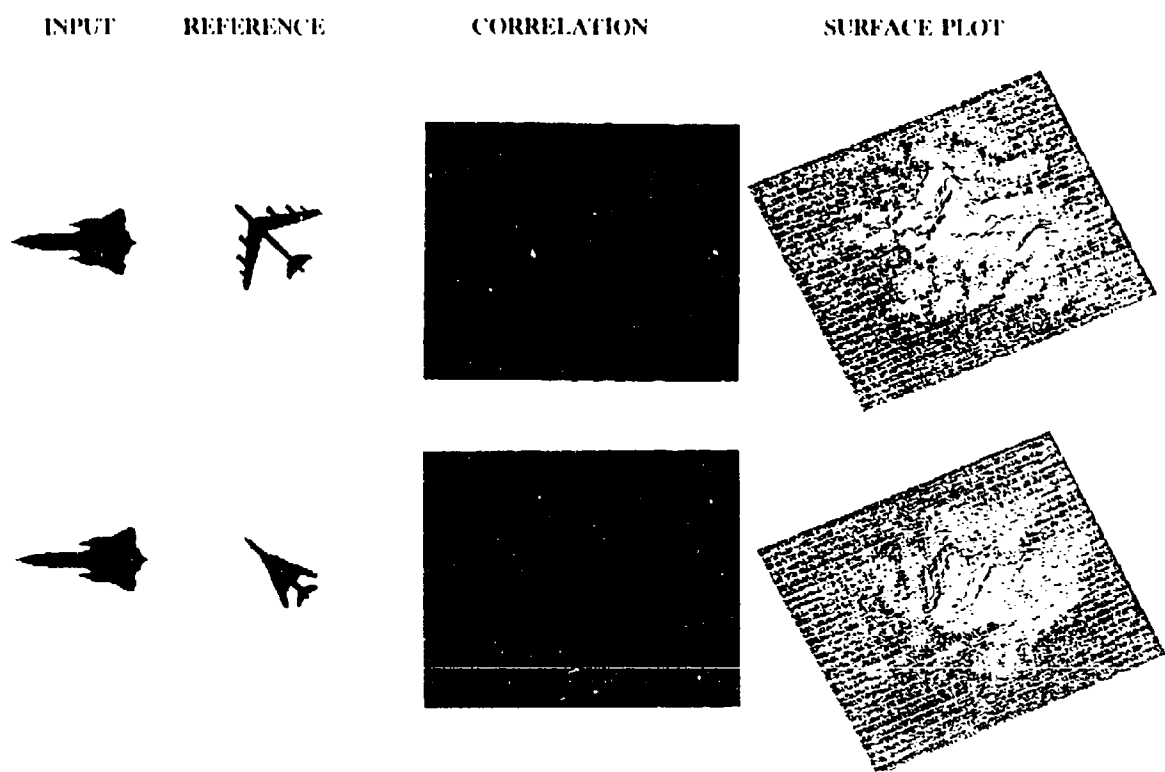


FIGURE 11 Optical image correlation experiment results, showing additional cross-correlation results.

With the 8 mm thick crystal (where FWHM was 0.125 Å), wavelength separations as close as 0.5 Å were investigated to take advantage of the narrower bandwidth and lower crosstalk features of the thicker holograms.

### TRANSLATION INVARIANCE

One of the advantages described earlier for orthogonal data storage holograms was their wide fields of view over non-counterpropagating reflection or transmission mode holograms. In the correlator application, where holograms are stored in the form of Fourier transforms, this angular tolerance is converted to translation or position invariance in the object plane.

Figure 12 illustrates the effect of input image translation in the optical correlator. For the 4 mm thick hologram at 650 nm, the angular field of view was calculated to be about  $2^\circ$ , which with the 85 mm focal length of the lens translates to a input plane position tolerance of 1.5 mm. To verify this property experimentally, a hologram was written in the crystal, the correlator was aligned, and the motion control system was used to move the input image slide while the correlation output spatial distribution and output power were recorded. Figures 13 and 14 show the output power and spatial distribution of the correlation peak, respectively, as a function of slide position  $\Delta x$ . The wide field of view of the hologram is reflected in the large  $\Delta x$  necessary to obtain a significant drop in auto-correlation efficiency.

In contrast, for the case of transmission mode holograms, the angular field of view of the gratings is considerably less than with orthogonal data storage. In a previous example, the theoretical field of view for a  $45^\circ$  incidence transmission mode grating is

## OPTICAL CORRELATOR WITH TRANSLATED IMAGE

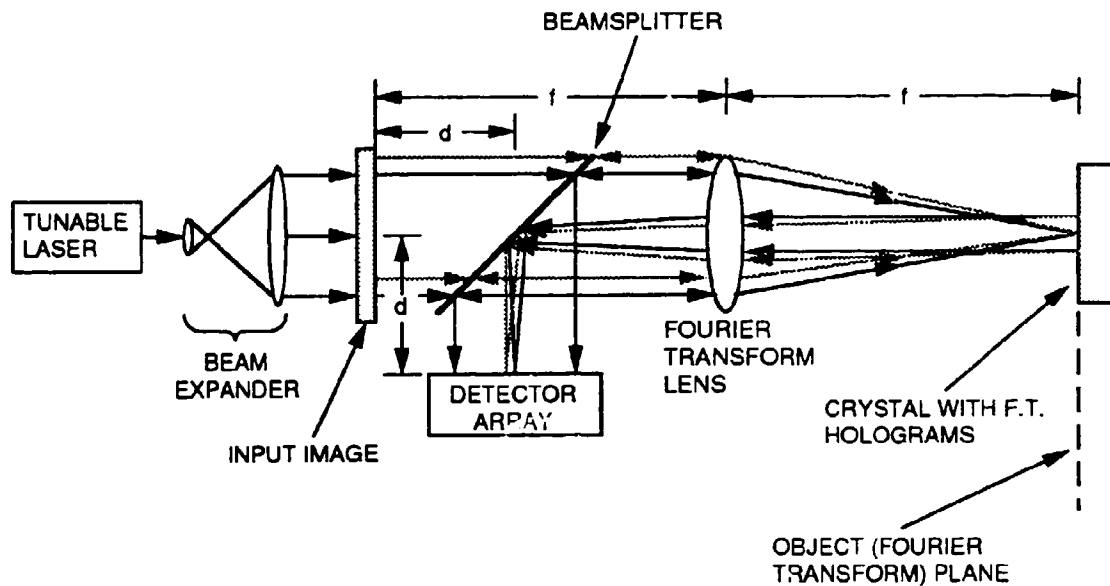


**FIGURE 12** Schematic diagram of the optical correlator for demonstration of input image translation invariance, where a motion control system was used to introduce a linear shift in the input image position to determine its effect on the correlation output.

### Optical Correlator Image Position Dependence

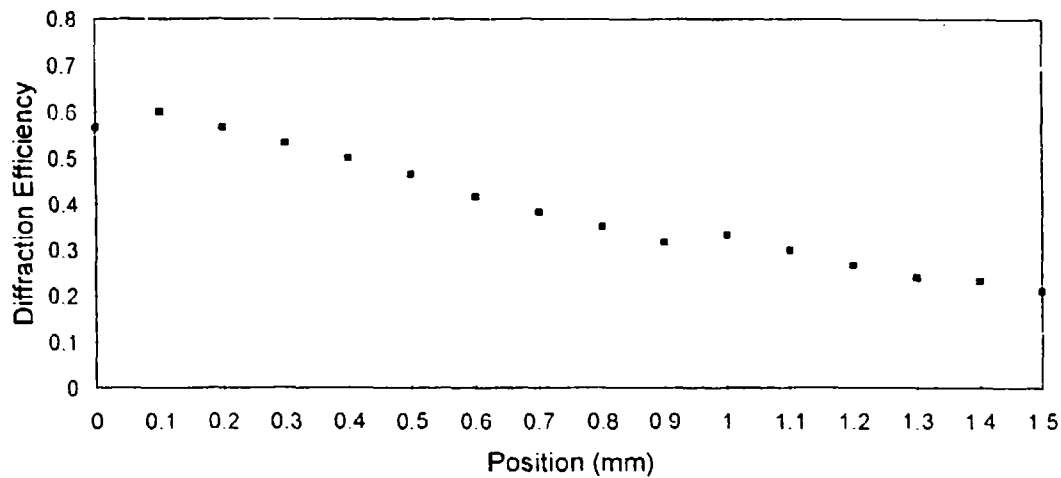


FIGURE 13 Auto-correlation efficiency of a single Fourier transform hologram as a function of input image translation.

### OPTICAL CORRELATOR TRANSLATION INVARIANCE

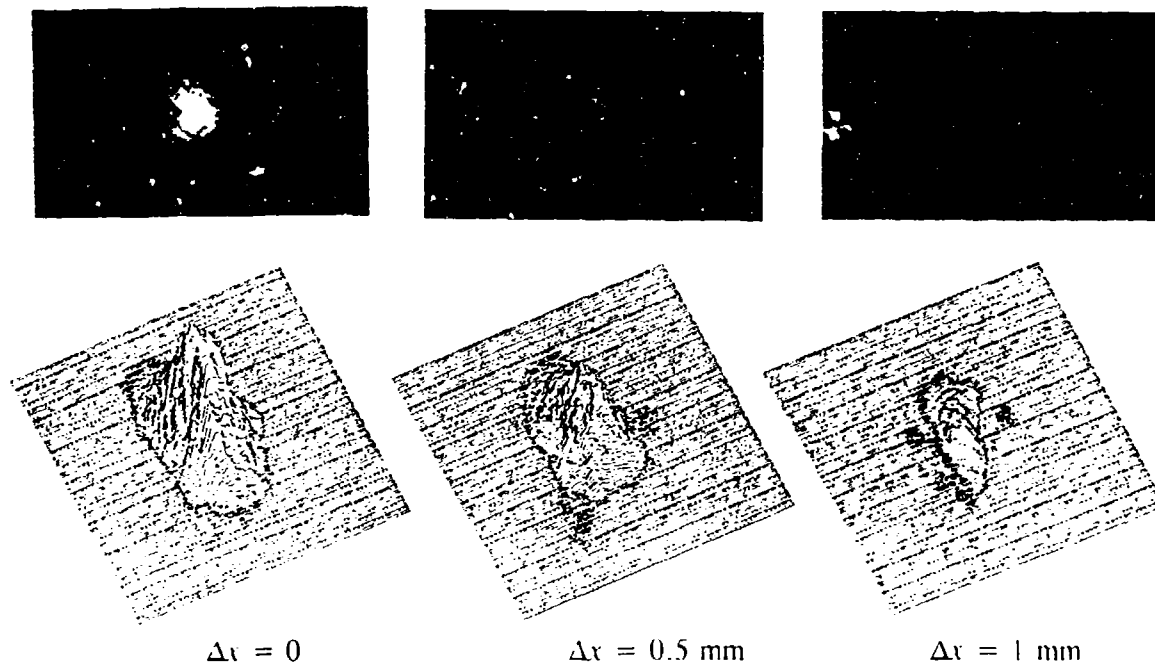


FIGURE 14 Effect of input image translation on the spatial distribution of the auto-correlation peak--note that it is approximately unchanged.

34", which corresponds to an input plane position tolerance of  $\pm 7 \mu\text{m}$  with the 85 mm Fourier transform lens.

### PARTIAL INPUTS

Another experiment that was performed with the correlator system was to test the effect of using partial (i.e. incomplete) input images during readout. In contrast with the case of using mismatched images, all of the rays that are incident on the crystal will still be Bragg-matched to the grating. Therefore, the spatial distribution of the correlation output should be unchanged, although the output signal amplitude will be lower because of the shadowed input image.

Figure 15 illustrates the results of an experiment to determine the effect of using partial input images in the optical correlator. The correlator was aligned, and the wavelength was set so the auto-correlation output was obtained for the selected input object. Then, various percentages of the input image were masked to determine the effect on the auto-correlation output. As one can see from Figure 15, the amplitude of the output is reduced, but the spatial distribution remains unchanged.

### **DISCUSSION**

Key technical issues relating to the integration of orthogonal data storage volume holography in optical image correlation have been investigated and addressed in this program. A breadboard correlator system using a holographic memory for reference templates has been set up and demonstrated at the Rome Laboratory Photonics Center. Auto- and cross-correlation outputs, translation invariance, and readout using incomplete images have also been demonstrated.

# CORRELATION--PARTIAL INPUT IMAGES

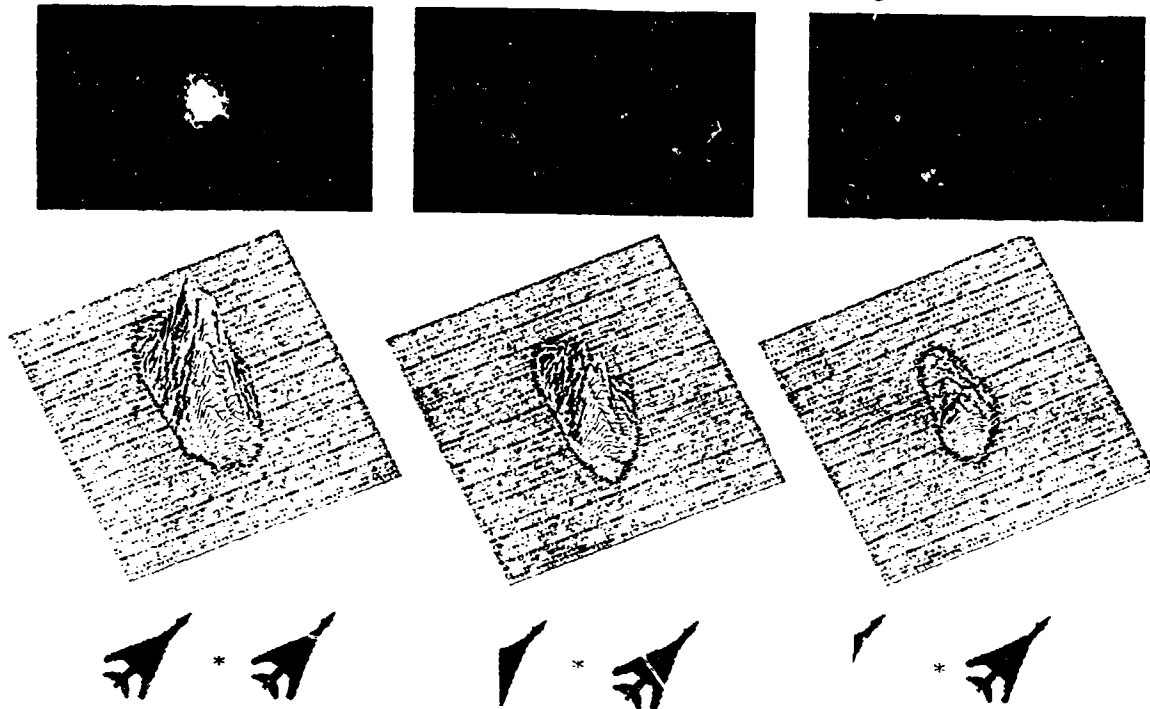


FIGURE 15 Effect of partial input images on the auto-correlation result.

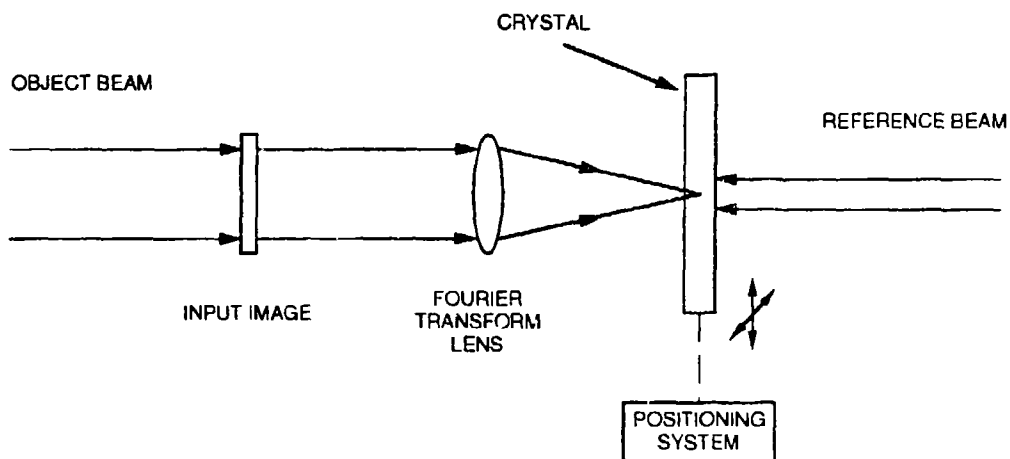


FIGURE 16 Method for taking advantage of the small area of the holograms by arraying multiple holograms across the surface of a large crystal.

For increased capacity, one can take advantage of the small surface area occupied by the holograms and the high spatial resolution feature of orthogonal data storage to array several sets of wavelength-multiplexed gratings across the face of a large crystal. These can then be addressed by using an automated positioning system as shown in schematic form in Figure 16. Using a thicker crystal to reduce the wavelength separation is another possible method to increase the number of holograms stored within the tuning range of the readout source.

In future work, the incorporation of a spatial light modulator (SLM) based image input, both for writing and readout, is one of the final elements necessary for a portable and operational system. Low throughput of the Semetek SLM currently in use at Rome Laboratory precluded its use in this current demonstration, particularly with a low power semiconductor laser. However, higher throughput devices with approximately 20% transmission,  $128 \times 128$  pixel resolution, and 4 mm array size have recently become available.<sup>15</sup> These SLM's are possible candidates for future use with this optical correlator system.

## PUBLICATIONS AND PRESENTATIONS

1. K. Sayano, G.A. Rakuljic, and G. Brost, "Translation invariant optical image correlator using orthogonal data storage," in preparation (1994).
2. K. Sayano, G.A. Rakuljic, and G. Brost, "Demonstration of a compact, random access optical image correlator an using orthogonal data storage holographic memory," submitted to Opt. Lett. (1994).
3. K. Sayano, G.A. Rakuljic, and G. Brost, "Compact optical image correlator using orthogonal wavelength multiplexed volume holograms," paper CTu-04, Conference on Lasers and Electro-Optics '94, Anaheim, CA (1994).
4. K. Sayano, G.A. Rakuljic, and G. Brost, "Optical image correlation using orthogonal wavelength multiplexed holograms," paper 2216-31, (Invited Paper), SPIE Optical Engineering in Aerospace Sensing, Orlando FL (1994).
5. K. Sayano, G.A. Rakuljic, and G. Brost, "Compact, fast access optical image correlator using orthogonal data storage," (Postdeadline), paper PDP-8, OSA Annual Meeting, Toronto (1993).

## REFERENCES

1. S.P. Kozaitis, S. Halby, and W. Foor, "Experimental performance of the binary phase-only optical correlator using visible and infrared imagery," Proc. SPIE vol. 1296, pp. 140-151 (1990).
2. J.L. Horner, B. Javidi, and J. Walkup, "Optical pattern system for verifying the authenticity of a person, product, or thing," AF Document #21069 (1993).
3. B. Javidi and J.L. Horner, "Optical pattern recognition for validity and security verification," paper 2237-27, SPIE Optical Engineering in Aerospace Sensing, Orlando, FL (1994).
4. J. Rosen, T. Kotzer, and J. Shamir, "Optical implementation of phase extraction pattern recognition," Opt. Commun. vol. 83, pp. 10-14 (1991).
5. K.H. Fielding, J.L. Horner, and C.K. Makekau, "Optical fingerprint identification by binary joint transform correlation," Opt. Eng. vol. 30, pp. 1958-1961 (1991).
6. A.B. VanderLugt, IEEE Trans. Inf. Theory IT-10, 139 (1964).
7. J.W. Goodman, Fourier Optics (New York, McGraw-Hill, 1968).
8. K. Sayano, G.A. Rakuljic, and G. Brost, "Compact, fast access optical image correlator using orthogonal data storage," paper PDP-8, Annual Meeting, Optical Society of America, Toronto, Canada (1993).
9. G.A. Rakuljic, V. Leyva, and A. Yariv, "Optical data storage by using orthogonal wavelength-multiplexed volume holograms," Opt. Lett. vol. 17, pp. 1471-1473 (1992).
10. G.A. Rakuljic and V. Leyva, "Materials for Orthogonal Data Storage," Final Report, Contract No. DAAH01-92-C-R303 (Accuwave Corporation, Santa Monica, CA, Dec. 1992).
11. M.G. Moharam, "Crosstalk in multiplexed volume holograms," paper WT-1, Annual Meeting, Optical Society of America, Albuquerque, NM (1992).
12. K. Curtis, C. Gu, and D. Psaltis, "Crosstalk in wavelength-multiplexed holographic memories," Opt. Lett. vol. 18, pp. 1001-1003 (1993).
13. G.A. Rakuljic and V. Leyva, "Volume holographic narrow-band optical filter," Opt. Lett. vol. 18, pp. 459-461 (1993).

14. H. Kogelnik, "Coupled wave theory for thick hologram gratings," Bell Syst. Tech. J. vol. 9, pp. 2909-2947 (1969).
15. Boulder Nonlinear Systems, Boulder, Colorado.